doi:10.1016/j.jmb.2005.09.042 J. Mol. Biol. (2005) 354, 403–412

JMB

Available online at www.sciencedirect.com

SCIENCE DIRECT®

ELSEVIER

Substrate Access to the Active Sites in Aminopeptidase T, a Representative of a New Metallopeptidase Clan

Sergey G. Odintsov[1,2,3], Izabela Sabała[1,2], Gleb Bourenkov[4], Vladimir Rybin[5] and Matthias Bochtler[1,2]*

[1]*International Institute of Molecular and Cell Biology ul. Trojdena 4, 02-109 Warsaw Poland*

[2]*Max-Planck-Institute for Molecular Cell Biology and Genetics, Pfotenhauerstr. 108 01309 Dresden, Germany*

[3]*Research and Production Center for Hematology and Transfusiology, Ministry of Health, Belarus 160 Dolginovsky Tract, 220053 Minsk, Belarus*

[4]*Max-Planck-Arbeitsgruppen für Strukturelle Molekularbiologie, Notkestr. 85 c/o DESY, 22607 Hamburg Germany*

[5]*European Molecular Biology Laboratory, Meyerhofstr. 1 69117 Heidelberg, Germany*

**Corresponding author*

Aminopeptidase T (AmpT) from *Thermus thermophilus* is a metallo-exopeptidase with no similarity to prototypical metallopeptidases with an HExxH or HxxEH motif. The crystal structure of the *Staphylococcus aureus* homologue of AmpT, which is known as aminopeptidase S (AmpS), has been reported recently. This structure revealed a dimeric protein with a very unusual, elongated shape and a large internal cavity. The active sites were found on the inner walls of the cavity and were entirely shielded from the environment, which suggested either that the dimer in the crystals was not physiologically relevant, or that an inactive conformation had been crystallized. Here, we show by gel-filtration and analytical ultracentrifugation that AmpT, like AmpS, forms dimers in solution, and we present the structure of AmpT in a crystal form with five protomers in the asymmetric unit. The five protomers take conformations that range from fully closed, as in the AmpS structure, to nearly open, so that the active site is almost directly accessible. The different conformations indicate flexibility between the AmpT N and C-domains, and explain how AmpT can be active, although the unusual AmpS dimerization mode applies to AmpT as well.

Keywords: protease; peptidase; metallopeptidase; aminopeptidase; crystal structure

Introduction

Aminopeptidase T (AmpT) from *Thermus thermophilus* has never been characterized biochemically, but many of its properties can be inferred from experimental data for closely homologous enzymes from other sources. The highly similar metallopeptidase AmpT from *Thermus aquaticus* (a) dimerizes in solution, (b) acts as an aminopeptidase and (c) requires metal cations, ideally Co^{2+}, for activity.[1,2] The *Bacillus stearothermophilus* AmpT homologue binds 2.2 cobalt ions per protomer according to equilibrium dialysis,[3] and the *Staphylococcus aureus* enzyme, known as AmpS, has two fully and one partially occupied metal binding site per protomer according to a recent crystal structure.[4]

AmpT and closely related peptidases (also known as MEROPS family M29 peptidases) do not resemble "standard" metallopeptidases with an H-E-x-x-H or H-x-x-E-H motif in sequence or structure, and have therefore recently been grouped together in the new MEROPS peptidase clan MQ. Structural information on clan MQ peptidases is so far based exclusively on the crystal structure of AmpS. This structure showed a very elongated dimer with active sites at opposite ends of a large internal cavity that was entirely inaccessible from outside. Therefore, it was clear that the AmpS structure could not represent the active enzyme.[4]

Several explanations for the lack of accessibility of the active sites in the AmpS dimer were considered: (a) the dimer may dissociate in solution,

Abbreviations used: AmpT, aminopeptidase T; MAD, multi-wavelength anomalous diffraction.

E-mail address of the corresponding author: mbochtler@iimcb.gov.pl

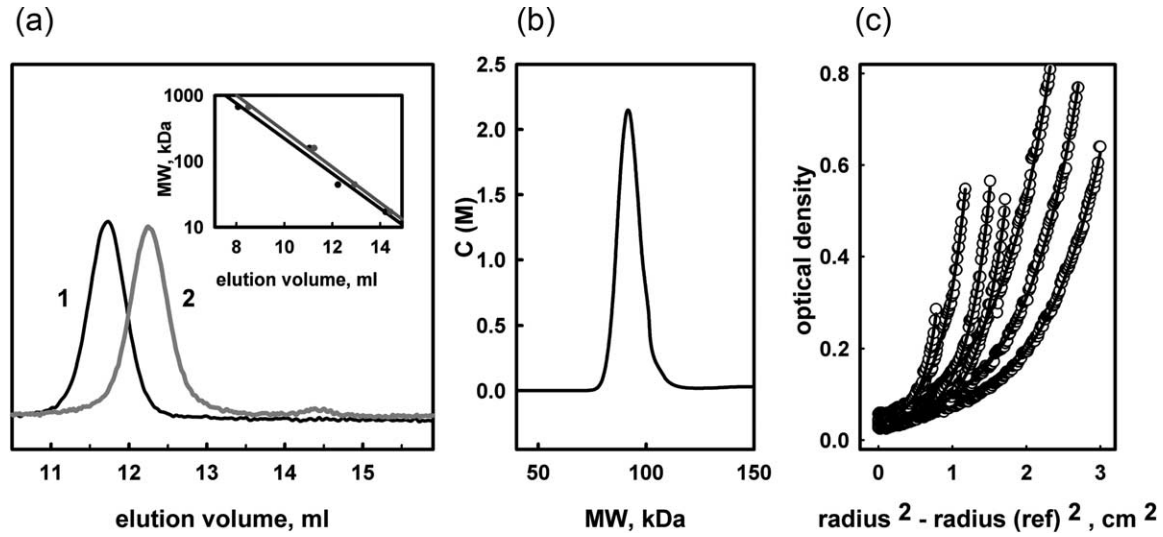

Figure 1. (a) Analytical gel-filtration profiles of AmpT after injection of 10 μg of AmpT into a Superose12 HR column. The black (1) and grey (2) UV traces were obtained in low-salt (10 mM Tris–HCl (pH 7.5), 50 mM NaCl) and high-salt (10 mM Tris–HCl (pH 7.5), 200 mM NaCl) running buffer, respectively. Separate calibration curves are presented for low-salt (black) and high-salt (grey) buffers. (b) Distribution of molecular mass according to a sedimentation velocity experiment run with 15 μM AmpT in high salt (10 mM Tris–HCl (pH 7.5), 200 mM NaCl). (c) Overlay of data (points) and fitted curves (lines) for sedimentation equilibrium experiments run in high-salt buffer (10 mM Tris–HCl (pH 7.5), 200 mM NaCl) with different centrifugation speeds and loading concentrations. The experimentally obtained profiles were fit with a monomer–dimer equilibrium model and a single set of parameters (global fitting).

and a small amount of the more accessible monomer may be the active species; (b) the biologically relevant dimer may not be present in the crystals, or may not have been assigned correctly; (c) the biologically relevant dimer may have crystallized, but domain movements may be required to allow access to the active sites. The biochemical and crystallographic data for AmpS suggested the latter possibility, but because the AmpS crystals contained only one protomer in the asymmetric unit, they could provide no direct evidence for conformational variability.[4]

Here, we present a biochemical characterization of AmpT and a crystal form of AmpT with five protomers in the asymmetric unit. Our data indicate that AmpT, like AmpS, forms highly elongated dimers in solution, which are present also in the crystal. A superposition of the five protomers in the asymmetric unit indicates that AmpT can take many different conformations, from fully closed, as in the AmpS structure, to nearly open, with almost exposed active site. This domain movement is likely to be a key feature of AmpT and its homologues.

Results and Discussion

T. thermophilus AmpT association state in solution

The AmpT homologues from *T. aquaticus*, *B. stearothermophilus* and *S. aureus* all behave as dimers in gel-filtration and analytical ultracentrifugation experiments, so AmpT from *T. thermophilus* was expected to migrate as a dimer. This was tested by sizing chromatography and analytical ultracentrifugation.

Gel-filtration runs were done in low-salt (50 mM NaCl) and high-salt (200 mM NaCl) conditions, and the migration of AmpT was compared with the migration of a set of standard proteins. As the standards migrated slightly differently in low-salt and high-salt buffers, two separate calibration curves were recorded. We obtained molecular masses 78(±15) kDa and 71(±9) kDa under low-salt and high-salt conditions, respectively (Figure 1(a)). The results agreed better with the calculated molecular mass of the AmpT dimer (90 kDa) than with the mass of the monomer (45 kDa), but the agreement was not fully satisfactory.

Therefore, we next analyzed the association state of AmpT in 20 mM Tris–HCl (pH 7.5), 200 mM NaCl by sedimentation equilibrium and sedimentation velocity ultracentrifugation. A sedimentation velocity experiment run with 15 μM AmpT indicated that at this concentration the enzyme sedimented as a single peak with a molecular mass of 89.0 kDa, which is in excellent agreement with the calculated molecular mass of the AmpT dimer (Figure 1(b)). To determine the monomer–dimer association constant, equilibrium centrifugation runs were performed at different speeds and concentrations of protein. The results indicate a monomer molecular mass of 47 kDa and an association constant around $0.9\times10^{6}\,M^{-1}$. As the sensitivity of the optical system of the ultracentrifuge precluded sedimentation equilibrium runs at very low concentrations of protein, the determination of the association constant required interpolation, and therefore it remains possible

that the true affinity is higher than the indicated value (Figure 1(c)).

AmpT structure determination

Crystals of AmpT were grown in space group $P4_2$ and contained five protomers in the asymmetric unit. Probably because of the large unit cell, AmpT crystals diffracted very poorly in-house on a rotating anode X-ray source and to only 3.7 Å on beamline 6 (BW6) of the Deutsches Elektronen-Synchrotron (DESY). The structure was solved by three-wavelength anomalous diffraction at the zinc K-edge. In the early stages of the project, the dimetal centres could not be resolved due to the low resolution of the data, and the dispersive and anomalous differences were interpreted in terms of a heavy-atom model with only five sites, which were obtained with the SHELXD program. The phasing with these five sites resulted in poor maps, which could be improved by solvent-flattening and 5-fold averaging. The determination of initial NCS operators was based on the observation that the dimetal centres, which were unresolved at this stage, were approximately related by local 5_1 screw axes that ran parallel with, but not coincident with, the crystallographic 4_2 axes. From the outset, it was clear that exact local 5_1 screw axes and crystallographic 4_2 axes required conflicting 90° and 72° angles between interacting neighbours, and could therefore not coexist for perfect AmpT dimers. The packing is possible only because AmpT protomers consist of two domains, henceforth called the N and C-domains, which can take different relative orientations, and thus can break the local 2-fold symmetry of the AmpT dimers (Figure 2). With multi-domain averaging and individual, resolved zinc sites, maps of sufficient quality for iterative refinement and manual model building were obtained. In the later stages, structure determination was facilitated greatly by the availability of the much higher resolution diffraction data for the AmpT homologue AmpS.[4]

AmpT dimerization mode

All AmpT protomers in the asymmetric unit have their dimerization partners, with which they associate *via* their N-domains. Four of the five protomers associate with a crystallographically independent protomer, the fifth protomer forms a dimer with its own crystallographic symmetry mate, which explains how an odd number of protomers in the asymmetric unit can be organized in pairs (Figure 2). The dimerization mode is consistent for all AmpT molecules and essentially identical with the previously reported AmpS dimerization mode, and is therefore likely to be relevant also in solution, even though it leads to very elongated, oddly non-spherical molecules. This conclusion is supported by the usual criteria to distinguish biologically relevant from purely crystallographic interfaces. In each AmpT dimer, the interface extends over roughly 1500 Å^2, or buries around 2×1500 Å$^2=3000$ Å^2 of solvent-accessible surface area, which is well within the range of biologically relevant protein contacts.[5] Moreover, the DFIRE (distance-scaled, finite, ideal-gas reference state) server,[6] which uses atom-based potentials to evaluate protein interfaces, classifies the described dimer contact as a "true interface", with a predicted dimer affinity around −25 kcal/mol. This theoretical value suggests an even tighter association than the analytical ultracentrifugation results, and provides strong support for the physiological relevance of the suggested dimer.

AmpT protomer structure

The AmpT protomer, like the AmpS protomer, can be divided into an N-terminal domain and a C-terminal domain. In the case of AmpT, which is from a hyperthermophilic organism and therefore more compact than *S. aureus* AmpS, the N-domain comprises residues 1–182 and the C-domain consists of residues 183–408. The most striking feature

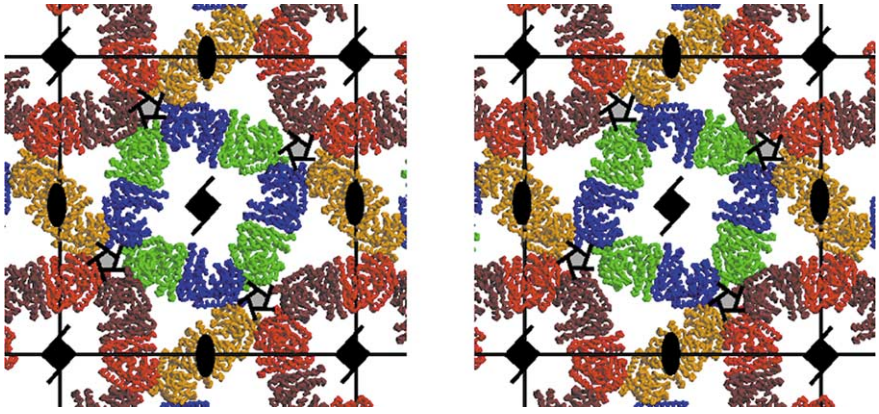

Figure 2. Crystal packing of AmpT. A stereo view along the crystallographic 4_2 axes and the local 5_1 axes is presented. The crystallographically independent protomers are coloured in green (chain A), blue (chain B), yellow (chain C), red (chain D) and brown (chain E). The green and blue subunits associate with biologically relevant dimers, and the same is true for the red and brown subunits. Yellow subunits associate with crystallographic symmetry mates to form exact dimers.

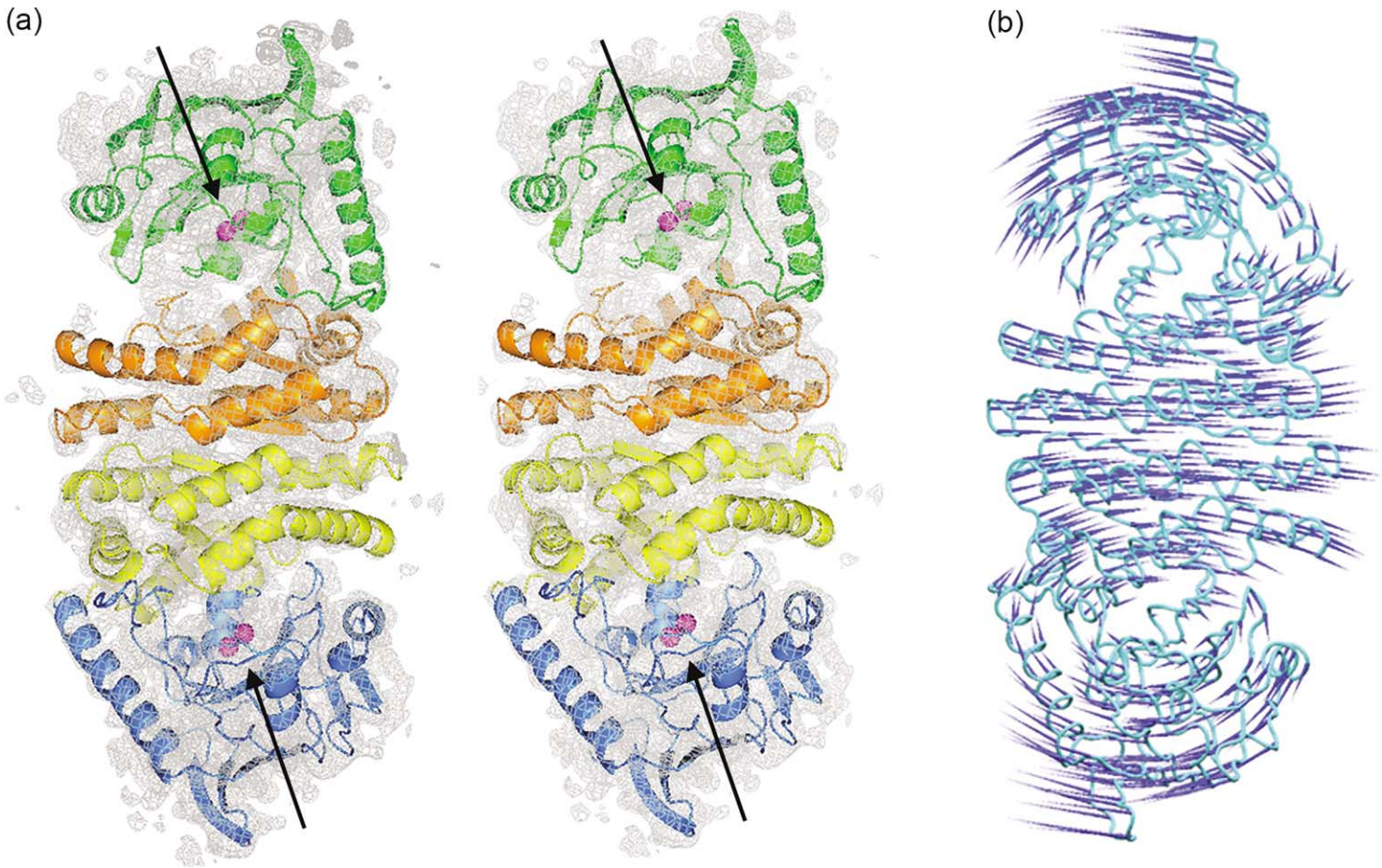

Figure 3. (a) Stereo representation of an AmpT dimer in the crystal. The N-domains are orange and yellow; the C-domains are green and marine. The zinc atoms are shown as pink spheres. The Figure has been created from suitably chosen symmetry mates of the protomers with segment identities D and E in the deposited PDB file. The original, experimental map after solvent flattening and averaging is contoured at 1σ and overlaid as a grey mesh. (b) Dynamite porcupine plot of the third principle mode of conformational variability.

of the AmpT dimers is the flexibility of the hinge region between the N and C-domains. With the exception of one protomer in the asymmetric unit, which dimerizes with a crystallographic symmetry mate, this results in AmpT dimers that follow the 2-fold symmetry in their N-domains, but not in the C-domains, which depend on the environment in the crystal for precise orientation. As a result, the accessibility of the active sites of the protomers in the "mixed" dimers is not equal, as illustrated by the example in Figure 3(a). The protomer at the bottom is in an entirely "closed" conformation, which shields the active site completely from the environment. In contrast, the protomer at the top is much more "open", so that the active site becomes almost accessible (Figure 3).

A range of conformations

Based on the results above, it could be expected that AmpT assumes a "closed" and an "open" conformation, and that the protein is always in one of two states, which would be stabilized by specific, but distinct patterns of contacts. The superposition of all independent AmpT protomer models shows that this is not the case, because the five protomers in the asymmetric unit sample different conformations and no single conformation occurs in duplicate (Figure 4(a)). The most closed AmpT conformation is similar to the previously reported AmpS conformation and yields a good superposition, without any adjustment of the hinge angle (Figure 4(b)).

Modelling supports the relevance of the domain motions

The protomer conformations in the crystal are necessarily influenced by crystal packing effects. In principle, molecular dynamics calculations could be used to independently verify domain motions, but for a molecule the size of the AmpT dimer, such simulations are computationally expensive, and non-Newtonian methods of ensemble generation are preferable. We used the Dynamite web-server,[7] which uses the CONCOORD program to generate distance-based ensembles and to analyze conformational variability.[8] We submitted the AmpT dimer with exact crystallographic 2-fold symmetry as the starting model to avoid introducing "hidden" crystallographic information about domain motion into the simulation. The metal ions had to be omitted, because they were not handled by the server. As they are anchored exclusively by the C-domains and do not mediate inter-domain contacts, this should not be a major limitation. The results from the server are presented in terms of so-called covariance webs, which connect atoms that move in concert with a correlation above a fixed threshold. In the case of AmpT, these connectivity maps show that the N and C-domains of AmpT are rather compact, but mobile with respect to each other (data not shown). Three dominant eigenmodes are identified by principle component analysis. The third such eigenmode corresponds to the "opening" and "closing" motion that is suggested by the crystallographic data (Figure 3(b)). The two other eigenmodes are not related to the conformational variability in the AmpT crystals (not shown).

Active site

The amino acid sequences of AmpT and AmpS are 40% identical, and all metal ligands in AmpS are also present in AmpT. We expect that the metal coordination in the two proteins is identical,

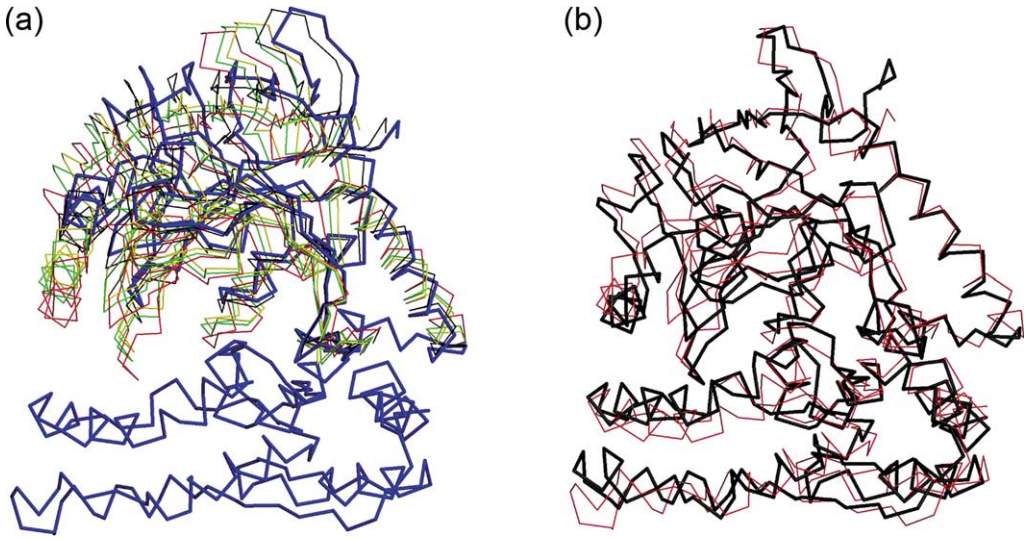

Figure 4. (a) Superposition of the five protomers based on a least-squares fit of the N-domains. The blue, brown, yellow, green and red protomers have segment identifiers B, E, C, A, D in the deposited PDB file. (b) Superposition of the C^{α} traces of AmpT (red lines, protomer D) and AmpS (black lines).

and that the AmpS-based homology model for this region is more accurate than the actual AmpT crystal structure, unless constraints from the model are used in the refinement. In AmpT numbering, we predict that Glu316 and possibly a water molecule serve as bridging ligands for both metal ions. We further expect that one of the metal ions is coordinated additionally by Asp378 and His376, and the other metal ion by Glu250 and His345. The deposited AmpT model, which was refined without model-based constraints, is compatible with these predictions, but the unconstrained metal–ligand distances are, of course, unreliable (data not shown).

Metal ion identity

T. aquaticus AmpT from the native source has been reported to contain Co ions, but Zn ions support the activity as well.[9] Therefore, the stronger Zn^{2+} and weaker Co^{2+} signal in an X-ray fluorescence scan of the *T. thermophilus* AmpT crystals was unexpected. Both the success of the multi-wavelength anomalous diffraction (MAD)-phasing procedure at the K-edge of zinc and the refined values for the real and imaginary parts of the metal scattering factors (see Materials and Methods) ruled out the possibility that the predominance of Zn^{2+} in the fluorescence scan was due to unspecifically bound metal. We conclude that Zn^{2+} was more abundant than Co^{2+} in the active sites, even though the significant anomalous signal in the 1.3000 Å data would be consistent with a minority fraction of Co ions in the active sites. The reason for the preferential incorporation of Zn^{2+} is not clear, but could be related to the purification from a recombinant source or the pre-treatment of the sample. We note also that a contamination of the $CaCl_2$ in the crystallization buffer at the 0.01% to 0.1% level would be sufficient to affect the balance of deliberately added Co and Zn ions.

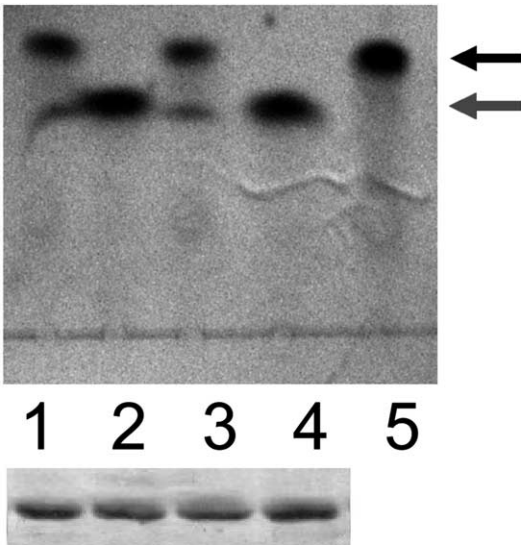

Figure 5. Comparison of the activities of AmpT in the crystals and in solution. The peptide Met-enkephalin was used as a substrate, and its degradation was monitored by thin-layer chromatography (TLC, upper panel). The black arrow points to uncleaved Met-enkephalin (applied in lane 5 as a standard), and the grey arrow indicates the degradation product. Two different buffer systems were used: the original crystallization buffer (0.1 M Tris–HCl (pH 8.5), 0.2 M $CaCl_2$, lanes 1 and 2) and a low-salt buffer (10 mM Tris–HCl (pH 7.5), lanes 3 and 4). Met-enkephalin was degraded less efficiently by AmpT in the crystals (lanes 1 and 3) than by AmpT in solution (lanes 2 and 4). The denaturing, Coomassie brilliant blue-stained SDS/polyacrylamide gel (lower panel) shows that equivalent amounts of protein were used for the comparisons.

Active site accessibility

The active site is entirely inaccessible in the more closed protomers, and almost accessible in the most open protomer of AmpT. This finding prompted us to compare the activities of equimolar amounts of AmpT in the crystals and in solution. The assays were done in crystallization buffer and repeated in standard assay buffer (10 mM Tris–HCl, pH 7.5) after pre-treatment of the crystals with glutaraldehyde (Figure 5). In both comparisons, the activity of the crystals turned out to be very low compared to the activity in solution. This may be due to impeded diffusion of the substrates and products within the crystals or could be due to limited conformational flexibility of the proteins within the crystal lattice. Alternatively, more open conformations than currently observed in the crystals could occur in solution and be responsible for most of the activity, especially at the high physiological temperatures for *T. thermophilus* around 75 °C. We note that the hinge region between the N and C-domains in the AmpT crystals is among the better conserved regions in the molecule. Therefore, it is likely that domain motion such as the motion described here could also control the active site access to other AmpT homologues, in particular to AmpS, which should otherwise not be proteolytically active.

Materials and Methods

AmpT cloning and expression

The standard PCR methods were used to amplify *ampT* from *T. thermophilus* and to clone it into pET15bmod, a variant of pET15b (Novagen) without the original EcoRI site. *Escherichia coli* BL21 (DE3) RIL cells were transformed with the plasmid and grown in LB medium containing 100 mg/l of ampicillin at 37 °C until the A_{600} reached 0.7. Then IPTG was added to a final concentration of 1 mM and cells were incubated for the next 5–6 h at 30 °C. Cells were harvested by low-speed centrifugation (4000 rpm for 10 min), resuspended in buffer A (10 mM Tris–HCl (pH 7.5), 100 mM NaCl, 10 μM $ZnCl_2$, 10 μM $CoCl_2$), and stored in aliquots at −20 °C. After thawing, cells were disintegrated by sonication.

Table 1. MAD data collection and phasing statistics

Space group		$P4_2$		
Unit cell dimensions				
a (Å)		246.5		
b (Å)		246.5		
c (Å)		51.1		
Matthews coeff (Å^3/Da)		3.4		
Solvent content (%, v/v)		63		
Resolution (last shell) (Å)	40.0–4.0 (4.05–4.00)	40.0–4.0 (4.05–4.00)	40.0–4.0 (4.05–4.00)	20–3.7 (3.9–3.7)
Wavelength (Å)	1.2780	1.2830	1.3000	1.2830
Total measured reflections	357,250	259,662	110,861	182,103
Unique reflections (Bijvoet pairs merged)	26,691	26,509	26,305	32,955
Completeness (last shell) (%)	100.0 (100.0)	98.5 (99.9)	94.2 (95.2)	97.9 (94.7)
I/σ (last shell)	31 (8)	25 (7)	16 (3)	8.4 (2.9)
R_{sym} (last shell) (%)	7.1 (17.8)	6.6 (17.7)	7.2 (27.2)	5.1 (18.4)
FOM (SHARP, ten sites)		0.42		–
NCS correlation after SHARP (domain 1/domain 2)		0.50/0.56		–
NCS correlation after dm (solvent flattening and averaging) (domain 1/domain 2)		0.89/0.90		–
FOM after dm (solvent flattening and averaging)		0.66		–
B(iso) from Wilson plot (Å^2)		91		

The inflection point wavelength was measured first. During data collection at this wavelength, the crystal acquired an ice ring. The first frames collected at this wavelength were processed separately to obtain a full-resolution dataset for refinement.

AmpT purification

The soluble fraction was clarified by ultracentrifugation at 50,000*g* for 30 min, heated to 80 °C for 30 min and then centrifuged to remove the precipitated proteins. The supernatant was applied to a DEAE-Sepharose FF column (Amersham Biosciences, 30 ml column volume) equilibrated in buffer A. The protein was recovered 90% pure in the flow-through, concentrated (Amicon 10 kDa cut-off regenerated cellulose filters), and loaded onto a Sephacryl S-300 HR (Amersham Biosciences) gel-filtration column in 5 mM Tris–HCl (pH 7.5).

Analytical FPLC

Size-exclusion analytical FPLC of AmpT was performed using the Ettan LC system on a prepacked Superose 12 HR 10/30 column (Amersham Biosciences). Two separate profiles were obtained for high-salt (10 mM Tris–HCl (pH 7.5), 200 mM NaCl) and low-salt (10 mM Tris–HCl (pH 7.5), 50 mM NaCl) running buffers. The column was calibrated with the following high molecular mass standards (Bio-Rad): thyroglobulin, 670 kDa; bovine γ-globulin, 158 kDa; chicken ovalbumin, 44 kDa; equine myoglobin, 17 kDa; vitamin B-12, 1.35 kDa.

Analytical ultracentrifugation

The oligomeric state of AmpT was investigated by monitoring its sedimentation properties in sedimentation velocity and equilibrium experiments. Sedimentation velocity profiles were collected by monitoring the absorbance signal at 280 nm as the samples were centrifuged at 55,000 rpm and 4 °C in a Beckman Optima XL-I centrifuge fitted with a four-hole AN-60 rotor and double-sector aluminium centrepieces. Sedimentation coefficient distributions were determined by the C(s) method implemented in the Sedfit software package.[10] Sedimentation equilibrium experiments were performed with a Beckman Optima XL-I centrifuge at 15,400 rpm, 23,000 rpm and 28,600 rpm, 4 °C and three different concentrations of protein (A_{280} 0.6, 0.4, and 0.2). Six-sector charcoal-Epon centrepieces were used. The data were analyzed using the program Global Fitting implemented in the Ultrascan 7.1 software package†. Buffer density and viscosity corrections were made according to the data published by Laue *et al.*,[11] as implemented in UltraScan. The partial specific volume was estimated from the protein sequence as described.[12]

AmpT crystallization

AmpT crystals were grown by the vapour-diffusion technique in sitting drops at 21 °C; 2 μl of protein solution was mixed with 2 μl of reservoir buffer and equilibrated against reservoir buffer. Tetragonal crystals were obtained with reservoir buffer B (0.1 M Tris–HCl (pH 8.5), 0.2 M $CaCl_2$) and could be flash-cryocooled in buffer B containing 15% (v/v) glycerol. Crystals belonged to space group $P4_2$ with cell constants $a=b=246.5$ Å, $c=51.1$ Å and contained five protomers in the asymmetric unit (Table 1).

Data collection

X-ray fluorescence measurements at beamline 6 (BW6) of the Deutsches Elektronen-Synchrotron (DESY) showed that the crystals contained more Zn^{2+} than Co^{2+}. Therefore, a MAD dataset was collected at the K-edge of zinc, at 100 K. The crystal diffracted originally to 3.7 Å, but acquired an ice-ring during data collection at the first wavelength. Although this ice ring limited the useful resolution of most frames to 4.0 Å, high-redundancy datasets were collected at the inflection point (1.2830 Å) and the absorption maximum (1.2780 Å), by rotation about a single fixed axis. In addition, a low-energy remote wavelength dataset (1.3000 Å) was recorded, primarily to

† http://www.ultrascan.uthscsa.edu

Table 2. Refinement statistics

Refinement statistics	
Reflections work/test	31,324/1629
Protein atoms	15,835
Metal ions	10
Water molecules	Not built
R-factor (%)	30.1
R_{free} (%)	32.1
rmsd from ideal	
Bond lengths (Å)	0.01
Bond angles (deg.)	1.4
NCS (Å), separate mappings for N and C-domains	0.02
Ramachandran plot	
Core region (%)	79.6
Allowed region (%)	18.9
Additionally allowed region (%)	1.5
Disallowed region (%)	0.0

check for a minority fraction of Co ions in the active site (see below). The diffraction data were integrated and scaled with DENZO and SCALEPACK, respectively. When the processing of the inflection point wavelength was limited to the frames that were not affected by the ice-ring problem, a dataset to 3.7 Å resolution was obtained that was better than all other, separately collected AmpT datasets (Table 1).

Structure determination

The SHELXD[13] software indicated that the signed anomalous differences for the absorption edge and inflection point datasets were significantly correlated up to about 5.0 Å (correlation between 0.75 and 0.50 for the resolution range from 8.0 Å to 5.0 Å). The program identified five confident sites (weights between 1.0 and 0.61 for the first five sites, weight 0.13 for the first "noise" peak), which later turned out to represent the unresolved dimetal centres. SHELXE[14] and SHARP[15] were used for phasing with these five sites. The contrast, a SHELXE measure of map quality related to the Terwillinger and Berendsen[16] criterion, clearly favoured one choice of hand over the enantiomorphic alternative (0.394 for the correct hand, and 0.178 for the incorrect hand after 20 cycles). Despite this difference, the maps were not interpretable and required averaging to improve phases (Table 1).

The determination of the non-crystallographic symmetry (NCS) operators for averaging was facilitated greatly by the observation that the SHELXD sites were arranged in regular intervals on spirals that ran parallel with the crystallographic 4_2 axes (not shown). The most parsimonious explanation for such a pattern, local 5_1 NCS-axes in the *c*-direction, was supported by significant density correlation and later turned out to be essentially correct, particularly for the C-domains close to the local axes (Figure 2). Starting from the 5_1 local screw symmetry, the NCS operators were refined and suitable monomer masks were defined. The dm[17] averaged and solvent-flattened map was of sufficient quality to build a C^{α} trace for about 75% of the 2040 residues of the five AmpT protomers, which was expanded to a polyalanine representation with the modelling program O.[18] When it became clear that AmpT protomers consisted of two domains that were trapped in different relative orientations in the crystals, multi-domain averaging and separate NCS restraints for the N and C-domains were introduced. With these improvements, iterative cycles of model building and structure refinement could have eventually led to an acceptable model.

At this stage, the availability of crystals of the AmpT homologue AmpS from *S. aureus* greatly facilitated structure determination. Unlike the AmpT crystals, the AmpS crystals contained only one protomer in the asymmetric unit and diffracted to high-resolution. Molecular replacement with the MOLREP[19] program was attempted with each of the five AmpT protomers as the search model, and worked best with the most closed AmpT protomer. The molecular replacement model was adjusted manually with the program O,[18] and then used for phase calculation. Starting from these model-based phases, ARP/WARP[20] delivered a nearly complete and almost fully refined AmpS structure (PDB accession code 1ZJC), which has been published separately.[4]

This AmpS protomer structure was then mapped back to the AmpT crystals, treating N and C-domains separately. This allowed us to confidently resolve the Zn^{2+} sites in each protomer. MAD phasing was repeated with the ten resolved sites, and phases were improved by solvent-flattening and averaging as before. Model fragments were adjusted manually to the experimental AmpT density, and served as the starting point for iterative cycles of model improvement, sequence correction, and refinement with standard NCS-restraints applied separately to the N and C-domains. The crystallography and NMR system (CNS)[21] was used with standard Engh and Huber parameters.[22] The quality indicators for the final model reflect the poor ordering of molecules in the crystal, which is evident from the high average *B*-factor of around 90 $Å^2$ according to the Wilson plot. Despite these limitations, the similarity between the uncertain AmpT structure and the confidently built AmpS structure indicates that at least the gross features of the AmpT model have to be correct (Table 2).

Refinement of the metal scattering factors

The real and imaginary parts of the scattering factors of the metal ions were determined with SHARP, in the case of the real part with reference to an arbitrarily chosen value for the real part at the remote wavelength. As the original SHARP phasing runs had too many free parameters, the runs were repeated with occupancies set to 1.0 and *B*-factors fixed at 91 $Å^2$, the average value of the temperature factor. All datasets were brought onto an absolute scale, and external model phases were imported into SHARP to aid the convergence of the refinement procedure. To avoid bias, the external phases for SHARP and their figures of merit were calculated for a model without metal ions. With this procedure, the imaginary parts of the scattering factors refined to $f''(1.2780\ Å) = 3.8 \pm 0.2$, $f''(1.2830\ Å) = 4.2 \pm 0.2$ and $f''(1.3000\ Å) = 1.6 \pm 0.2$. For the real parts of the scattering factors, we found $f'(1.2780\ Å) - f'(1.3000\ Å) = -1.1 \pm 0.3$ and $f'(1.2830\ Å) - f'(1.3000\ Å) = -3.8 \pm 0.3$, in generally good agreement with the expected values for Zn^{2+} according to the Sasaki tables, as quoted in SHARP:[15] ($f''(1.2780\ Å) = 3.9$, $f''(1.2830\ Å) = 3.9$, $f''(1.3000\ Å) = 0.5$, f' $(1.2780\ Å) - f'(1.3000\ Å) = -1.0$, f' $(1.2830\ Å) - f'(1.3000\ Å) = -3.5$). The high imaginary part of the scattering factor at 1.3000 Å could be due to a minority fraction of Co ions in the active sites.

Cross-linking of AmpT crystals

Without stabilization, crystals of AmpT did not survive transfer from the crystallization mother liquor to the standard assay buffer. Therefore, crystals were first transferred to a 20 µl drop that was mixed from 16 µl of crystallization reservoir buffer and 4 µl of 25% (v/v) glutaraldehyde stock in water. After cross-linking for 1 h, the crystals were washed several times in the original crystallization buffer and stored at room temperature.

Probing the AmpT crystals activity with Met-enkephalin

To test activity, the single AmpT crystal was incubated in a 3 µl drop, containing 5 µg (8.5 nmol) of Met-enkephalin (Tyr-Gly-Gly-Phe-Met) at 37 °C for 40 min. Two different buffer systems were used for the reactions: the original reservoir buffer B for the non-cross-linked crystals, and 10 mM Tris–HCl (pH 7.5) for the cross-linked crystals. The reaction was stopped with 10 mM EDTA and the samples were applied onto a thin-layer chromatography plate covered with Silica gel 60 F_{254} (Merck). The plate was developed with *n*-butanol/acetic acid/Milli-Q water (4:1:1 by vol.) and stained with ninhydrin. To compare the activity of AmpT in solution with the crystallized species, the equivalent amount of the soluble protein (approximately 20 pmol as judged by SDS-PAGE) was incubated with Met-enkephalin as described above. For all comparisons, the AmpT activity had to be assayed at 37 °C, because the crystals did not tolerate the higher temperatures, where AmpT activity is maximal.

Protein Data Bank accession code

The atomic coordinates and structure factors have been deposited in the Protein Data Bank, Research Collaboratory for Structural Bioinformatics, Rutgers University, New Brunswick, NJ†, with accession code 2AYI.

Acknowledgements

We thank Melanie Stefan for help with the biochemical work during a summer practicum and Professor Hans Bartunik for generous allocation of beamtime on BW6 (DESY, Hamburg). This work was supported by the Polish Ministry of Scientific Research and Information Technology (MNiI, decisions 1789/E-529/SPB/5.PR UE/DZ 600/2002-2005, 158/E-338/SPB/5.PR UE/DZ 19/2003 and KO89/PO4/2004) and by the Commission of the European Community, specific RTD program "Quality of Life and Management of Living Resources", QLRT-2001-01250, "Novel non-antibiotic treatment of staphylococcal diseases". M.B. thanks the European Molecular Biology Organization (EMBO) and the Howard Hughes Medical Institute (HHMI) for Young Investigator support.

† http://www.rcsb.org

References

1. Minagawa, E., Kaminogawa, S., Matsuzawa, H., Ohta, T. & Yamauchi, K. (1988). Isolation and characterization of a thermostable aminopeptidase (aminopeptidase T) from *Thermus aquaticus* YT-1, an extremely thermophilic bacterium. *Agric. Biol. Chem.* **52**, 1755–1759.
2. Motoshima, H. & Kaminogawa, S. (1998). Aminopeptiase T. In *Aminopeptidase II from Bacillus stearothermophilus* (Barrett, A. J., Rawlings, N. D. & Woessner, J., eds), pp. 1452–1454, Academic Press, London.
3. Stoll, E., Weder, H. G. & Zuber, H. (1976). Aminopeptidase II from *Bacillus stearothermophilus*. *Biochim. Biophys. Acta*, **438**, 213–220.
4. Odintsov, S. G., Sabala, I., Bourenkov, G., Rybin, V. & Bochtler, M. (2005). *Staphylococcus aureus* aminopeptidase S is a founding member of a new peptidase clan. *J. Biol. Chem.* **280**, 27792–27799.
5. Jones, S. & Thornton, J. M. (1996). Principles of protein–protein interactions. *Proc. Natl Acad. Sci. USA*, **93**, 13–20.
6. Zhou, H. & Zhou, Y. (2002). Distance-scaled, finite ideal-gas reference state improves structure-derived potentials of mean force for structure selection and stability prediction. *Protein Sci.* **11**, 2714–2726.
7. Barrett, C. P., Hall, B. A. & Noble, M. E. (2004). Dynamite: a simple way to gain insight into protein motions. *Acta Crystallog. sect. D*, **60**, 2280–2287.
8. de Groot, B. L., van Aalten, D. M., Scheek, R. M., Amadei, A., Vriend, G. & Berendsen, H. J. (1997). Prediction of protein conformational freedom from distance constraints. *Proteins: Struct. Funct. Genet.* **29**, 240–251.
9. Myrin, P. A. & Hofsten, B. V. (1974). Purification and metal ion activation of an aminopeptidase (aminopeptidase II) from *Bacillus stearothermophilus*. *Biochim. Biophys. Acta*, **350**, 13–25.
10. Schuck, P. (2000). Size-distribution analysis of macromolecules by sedimentation velocity ultracentrifugation and lamm equation modeling. *Biophys. J.* **78**, 1606–1619.
11. Laue, T. M., Shah, B. D., Ridgeway, T. M. & Pelletier, S. L. (1992). Computer-aided interpretation of analytical sedimentation data for proteins. In *Proteins, Amino Acids and Peptides* (Harding, S. E., Rowe, A. J. & Horton, J. C., eds), pp. 90–125, The Royal Society of Chemistry, Cambridge, UK.
12. Cohn, E. J. & Edsall, J. T. (1943). *Proteins, Amino Acids and Peptides*, Reinhold, New York.
13. Uson, I. & Sheldrick, G. M. (1999). Advances in direct methods for protein crystallography. *Curr. Opin. Struct. Biol.* **9**, 643–648.
14. Sheldrick, G. M. (2002). Macromolecular phasing with SHELXE. *Z. Kristallog.* **217**, 644–650.
15. Bricogne, G., Vonrhein, W., Paciorek, C., Flensburg, M., Schiltz, E., Blanc, P. *et al*. (2002). Enhancements in AUTOSHARP and SHARP with applications to difficult phasing problems. *Acta Crystallog. sect. A*, **58**, C239.
16. Terwilliger, T. C. & Berendzen, J. (1999). Discrimination of solvent from protein regions in native Fouriers as a means of evaluating heavy-atom solutions in the MIR and MAD methods. *Acta Crystallog. sect. D*, **55**, 501–505.
17. Collaborative Computational Project Number 4 (1994). The CCP4 suite: programs for protein crystallography. *Acta Crystallog. sect. D*, **50**, 760–763.

18. Jones, T. A., Zou, J. Y., Cowan, S. W. & Kjeldgaard, M. (1991). Improved methods for building protein models in electron density maps and the location of errors in these models. *Acta Crystallog. sect. A*, **47**, 110–119.
19. Vagin, A. & Teplyakov, A. (1997). MOLREP: an automated program for molecular replacement. *J. Appl. Crystallog.* **30**, 1022–1025.
20. Morris, R. J., Perrakis, A. & Lamzin, V. S. (2003). ARP/wARP and automatic interpretation of protein electron density maps. *Methods Enzymol.* **374**, 229–244.
21. Brunger, A. T., Adams, P. D., Clore, G. M., DeLano, W. L., Gros, P., Grosse-Kunstleve, R. W. *et al*. (1998). Crystallography and NMR system: a new software suite for macromolecular structure determination. *Acta Crystallog. sect. D*, **54**, 905–921.
22. Engh, R. A. & Huber, R. (1991). Accurate bond and angle parameters for X-ray protein structure refinement. *Acta Crystallog. sect. A*, **47**, 392–400.

Edited by R. Huber

(Received 10 July 2005; received in revised form 10 September 2005; accepted 14 September 2005)
Available online 30 September 2005